Materials Horizons

ROYAL SOCIETY OF CHEMISTRY

COMMUNICATION

Published on 13 July 2026

Cite this: DOI: 10.1039/d6mh00729e

Room-temperature electrical control of thermal conductivity in ZrO_2

Antonio Cappai, [a] Pol Benítez, [bc] Cibrán López, [bc] Claudio Cazorla [bcd] and Riccardo Rurali *[e]

Received 12th April 2026,
Accepted 9th July 2026

DOI: 10.1039/d6mh00729e

rsc.li/materials-horizons

The ability to dynamically tune the lattice thermal conductivity, *k*, of solids would enable real-time control of heat flux, a key requirement for emerging applications in phonon-based logic, thermal memories, and energy-harvesting technologies. For such schemes to become practical, thermal transport must be switchable through fast and experimentally accessible stimuli, such as electric or magnetic fields or light absorption. Here, using first-principles calculations, we demonstrate that the electric-field-induced antiferroelectric-to-ferroelectric phase transition in ZrO_2, where the crystal structure transforms from tetragonal to orthorhombic, provides an effective route to achieve this control. We show that higher-order anharmonic processes are essential to quantitatively describe both the absolute thermal conductivities of the two phases and their variations across the transition. Our results reveal an overall increase in *k* when nonpolar tetragonal ZrO_2 converts into its ferroelectric orthorhombic counterpart, with the largest modulation (≈50%) occurring along the long axis of the tetragonal/orthorhombic cell. This sizable and anisotropic thermal response offers a promising mechanism for designing electrically controlled thermal-management devices such as thermal memories and thermal transistors.

New concepts

The dynamical tuning of the thermal transport properties of materials can play an important role in a number of applications, ranging from smart thermal management (*e.g.*, selective cooling of hot spots) to the design of thermoelectric modules with adjustable figures of merit and heat scavengers compliant with varying environmental conditions. Here, we propose an all-electrical control of thermal conductivity by leveraging a structural phase transition in ZrO_2. We report a large ~50% change in the thermal conductivity upon field-induced antiferroelectric-to-ferroelectric phase transition. Importantly, this phase transition in ZrO_2 thin films has already been demonstrated experimentally and it is ultrafast and reversible. This makes our predictions well-suited for immediate experimental verification and paves the way for real-time control of the heat flux in solids.

1 Introduction

Many applications, from solid-state electronics to edge computing and energy harvesting, depend crucially on tight control of heat transfer. Nevertheless, our ability to manipulate phonons – the heat carriers in insulators and semiconductors – lags far behind what can be achieved with other particles,[1] such as electrons and photons, and heat is usually associated with losses and inefficiency. The design of materials with tailor-made thermal properties relies on the engineering of structural defects and nanostructuring, in order to create scattering centers for phonon transport. These approaches, nonetheless, at best yield modifications of the thermal conductivity that are static and irreversible. The dynamical modulation of the thermal conductivity, on the other hand, could provide enhanced capabilities in terms of heat transport control, allowing for heat guiding or for the selective cooling of hot spots, and would enable phonon-based logic,[2,3] where information is encoded with heat carriers.[4] To this aim, significant research efforts must be made to devise novel strategies that allow fast manipulation of phonons, leading to on-demand thermal properties.

Oxides play an important role in this field.[5] They are usually made of naturally abundant elements, are thermodynamically and structurally stable, and can exhibit very rich phase diagrams. Field-induced structural phase transitions, in particular, are very appealing for the design of thermal switches and thermal memory elements, because they can potentially provide relatively fast and accurate switching times and a high

[a] *Department of Physics, University of Cagliari, Monserrato, 09042 Cagliari, Italy*
[b] *Departament de Física, Universitat Politècnica de Catalunya, Campus Diagonal-Besòs, Av. Eduard Maristany 10–14, 08019 Barcelona, Spain*
[c] *Research Center in Multiscale Science and Engineering, Universitat Politècnica de Catalunya, Campus Diagonal-Besòs, Av. Eduard Maristany 10–14, 08019 Barcelona, Spain*
[d] *Institució Catalana de Recerca i Estudis Avançats (ICREA), Passeig Lluís Companys 23, 08010 Barcelona, Spain*
[e] *Institut de Ciència de Materials de Barcelona, ICMAB-CSIC, Campus UAB, 08193 Bellaterra, Spain. E-mail: rrurali@icmab.es*

contrast between the high- and low-conductivity states.[6,7] Zirconia (ZrO_2) is a material that fulfills many of these conditions. In particular, it presents an antiferroelectric → ferroelectric phase transition that can occur at room temperature, as both theoretically predicted[8] and experimentally observed,[9,10] and be triggered by external electric bias. In its bulk form and in the absence of external pressure, ZrO_2 exhibits three prominent structural phases: at high temperature, it is nonpolar and cubic (fluorite structure, space group $Fm\bar{3}m$); between 1200–1400 and 2750 K, it is tetragonal (space group $P4_2nmc$); and below 1200–1400 K, it is monoclinic (space group $P2_1/c$; see the SI). Nevertheless, in thin-films, the tetragonal–monoclinic transition temperature is suppressed and the room-temperature thermodynamically stable phase of ZrO_2 is tetragonal.[8,11–13] Zirconia has also a polar orthorhombic phase (space group $Pca2_1$), where ferroelectricity can be stabilized *via* epitaxial strain[8] or continuous substitution of Zr by Hf.[9,14] Recently, Lomenzo and coworkers[10] have demonstrated experimentally that the polar phase can also be accessed by means of an external electric field, more specifically *via* field-induced phase transition from the nonpolar, antiferroelectric tetragonal phase (tetra^{AFE}) to the ferroelectric orthorhombic phase (ortho^{FE}).

In this study, we leverage on the reversible tetra^{AFE} ↔ ortho^{FE} phase transition occurring at room temperature to propose a thermal switch capable of storing '0' and '1' *via* the low- and high-conductivity states of ZrO_2. For this, we compute within an entirely *ab initio* framework the lattice thermal conductivity, k, of both crystal phases. An additional reason of interest, more on the fundamental side of heat transport, is that zirconia is a prototypical anharmonic material[15,16] and thus predictive theoretical calculations are a challenge *per se*, as high-order anharmonic contributions must be accounted for.

2 Methods

We carried out density-functional theory calculations with the VASP package,[17–19] using an energy cutoff of 600 eV, the projector augmented wave method,[20] and the generalized gradient approximation PBEsol[21] for the exchange–correlation energy. The following electrons were explicitly treated as valence electrons: Zr $4s^24p^65s^24d^2$ and O $2s^22p^4$. We studied the tetra^{AFE} $P4_2nmc$ and the *ortho*^{FE} $Pca2_1$ crystal phases of ZrO_2, sampling the Brillouin zone with a grid of 12 × 12 × 9 and 9 × 9 × 9 k-points, respectively. We optimized the atomic positions and the lattice vectors until forces and stress were lower than 5×10^{-4} eV Å^{-1} and 1.5×10^{-2} kbar, respectively. We then computed the second-, third-, and fourth-order interatomic force constants (IFCs) by finite differences using phonopy,[22] thirdorder.py,[23] and fourthorder.py,[24] respectively. Second- and third-order IFCs were computed in a 4 × 4 × 3 (3 × 3 × 3) supercell for the tetra^{AFE} (ortho^{FE}) phase, neglecting interactions beyond 0.41 nm (equivalent to a cutoff to the 6th nearest neighbors for the tetra^{AFE} phase) in the case of anharmonic IFCs. Fourth-order IFCs were computed in a reduced 3 × 3 × 3 (2 × 2 × 2) supercell, for the tetra^{AFE} (ortho^{FE}) phase, with a cutoff up to 2nd neighbors.

These IFCs were then used as input to solve the linearized phonon Boltzmann Transport Equation (BTE) using FourPhonon,[24] an extension of the ShengBTE code[23] that can deal with phonon–phonon processes up to the 4th order. In our solution of the BTE, both three-phonon (3ph) and four-phonon (4ph) scattering processes are treated within the relaxation time approximation (RTA),[25] which proved to be an excellent approximation for room-temperature ZrO_2. Each $i, j = x, y, z$ Cartesian component of the lattice thermal conductivity tensor $\kappa_{ij}(T)$ at temperature T is calculated as a sum over all phonon modes λ and all N_q q-points inside the first Brillouin zone of the unit cell of the crystal with volume Ω as:

$$\begin{aligned}\kappa_{ij} &= \frac{1}{\Omega N_q}\sum_{\lambda}\sum_{q} f_{\lambda,q}\left(f_{\lambda,q}+1\right)\frac{(\hbar\omega_{\lambda,q})^2}{k_B T^2}\tau_{\lambda,q} v^i_{\lambda,q} v^j_{\lambda,q} \\ &= \frac{1}{N_q}\sum_{\lambda}\sum_{q} f_{\lambda,q}\left(f_{\lambda,q}+1\right) C_{\lambda,q}(T)\tau_{\lambda,q} v^i_{\lambda,q} v^j_{\lambda,q}\end{aligned} \quad (1)$$

where k_B and $\hbar$ represent, respectively, the Boltzmann constant and the reduced Planck constant, and $C_{\lambda,q}(T) = \frac{(\hbar\omega_{\lambda,q})^2}{\Omega k_B T^2}$ is directly related with the volumetric heat capacity $C_{V,\lambda}(T)$ of the phonon mode λ at temperature T according to $C_{V,\lambda}(T) = \sum_q C_{\lambda,q}(T)$.

The Cartesian components of the phonon group velocities $v^{i,j}_{\lambda,q}$ and the phonon lifetimes $\tau_{\lambda,q}$ are weighted according to the $f_{\lambda,q}$ equilibrium Bose–Einstein distribution function, running over all phonon modes and q-points of the first Brillouin zone. In particular, phonon velocities are directly obtained from harmonic IFCs, while third and fourth order IFCs dictate the magnitude of $\tau_{\lambda,q}$, as reported elsewhere. Isotopic scattering contributes as well to the phonon lifetimes, and was included assuming the natural abundances of Zr and O isotopes, and following the analytical treatment of the Tamura model.[26]

The phonon BTE was solved on a 7 × 7 × 5 (5 × 5 × 5) for the tetra^{AFE} (ortho^{FE}) crystal phase and employing a width of the Gaussian functions, $\sigma = 0.1\bar{\sigma}$, that are used to determine which phonon–phonon collisions conserve energy and momentum (being $\bar{\sigma}$ the default value in FourPhonon[23,24]). The choice of these parameters allowed us to greatly reduce the number of 3ph and 4ph processes, without compromising the accuracy of our results. Extensive convergence tests are reported in the SI.

Thermal conductivity tensors are reported in the crystallographic principal axes of each phase. The orthorhombic a- and b-axes correspond to the two diagonal directions of the tetragonal ab-plane, while the c-axis is common to the two phases. Since the tetragonal thermal conductivity tensor is isotropic within the basal plane, this 45-degree in-plane rotation does not affect the comparison of the in-plane components; the comparison along the c-axis, on the other hand, is direct.

3 Results and discussion

3.1 Thermal conductivity and role of higher-order anharmonicity

We start by modelling ZrO_2 in its tetragonal structure (space group $P4_2/nmc$), typically adopted in thin films and characterized by antiferroelectric (AFE) order. After structural optimization, we obtain lattice parameters of $a = b = 3.586$ Å and $c = 5.173$ Å. For the orthorhombic phase (space group $Pca2_1$), which is ferroelectric (FE) and can be stabilized by an electric field as demonstrated experimentally by Lomenzo and coworkers,[10] we obtain lattice parameters of $a = 5.053$ Å, $b = 5.072$ Å, and $c = 5.257$ Å. In both cases, our results are in very good agreement with the experimental values reported.[27–29]

The phonon dispersions of the two phases are shown in Fig. 1(a) and (b), where the clear absence of imaginary modes in both cases confirms their dynamical stability. The computed thermal conductivity is displayed in Fig. 1(c) and (d), where we plot the three diagonal components of the k tensor for both crystal phases. We verified that all off-diagonal components are negligible, as expected from the lattice underlying symmetry. We present results obtained by considering only three-phonon (3ph) scattering processes (yellow bars) alongside those including both three-phonon and four-phonon (4ph) scattering (orange bars).

As previously discussed by others,[15,16] ZrO_2 exhibits considerable anharmonicity, and higher-order anharmonic processes play an important role in determining its thermal transport properties. This effect is more pronounced in the tetragonal polymorph, where the thermal conductivity decreases by more than 30% when 4ph processes are included. In contrast, the orthorhombic phase exhibits a smaller reduction: 15% and 13% for κ_{xx} and κ_{yy}, respectively, while κ_{zz} remains nearly unaffected (4ph corrections below 8%), indicating that predictions based on 3ph scattering alone are already quite accurate for this component.

This behavior is straightforwardly explained by the phonon scattering rates, τ^{-1}, shown in Fig. 1(e) and (f). The 4ph scattering cross-sections are substantially larger for the tetragonal phase compared to the orthorhombic phase, particularly at low frequencies ($\omega \sim 5$ THz), where the phonons with high group velocities (carrying the largest fraction of the total heat flux) are present. Remarkably, 4ph scattering processes account for a dramatic reversal in the relative ordering of the average thermal conductivities. In fact, while $\langle\kappa_{\text{tetra}^{\text{AFE}}}\rangle > \langle\kappa_{\text{ortho}^{\text{FE}}}\rangle$ (where $\langle\cdots\rangle$ indicates the average value of k) at the 3ph level (7.5 *vs.* 6.8 W m^{-1} K^{-1}), this ordering is reversed when 4ph processes are included (5.1 *vs.* 6.0 W m^{-1} K^{-1}), demonstrating the critical importance of including higher-order anharmonicity in these polymorphs.

It is worth noting that the role of four-phonon scattering in determining lattice thermal conductivity has attracted significant attention in recent years, and it is now well established that, while not universally dominant, it can be crucial in materials with strong anharmonicity and/or at elevated temperatures. For instance, in silicon and diamond, the inclusion of four-phonon processes reduces the predicted thermal conductivity by approximately 30% at high temperatures, yielding excellent agreement with experiment.[30] Similar reductions of about 30% have been reported in layered oxyselenides such as Na_2CoSe_2O,[31] while even larger effects, ranging from ~30% up to 80%, have been observed in carbon-based materials like graphene and graphyne depending on temperature.[32,33] These examples, spanning diverse bonding environments and dimensionalities, demonstrate that strong four-phonon effects are a recurring feature in anharmonic systems rather than an exception. In this context, the distinct behavior observed here for the tetragonal and orthorhombic phases of ZrO_2 can be naturally attributed to differences in their anharmonic energy landscapes and available phonon phase space (see the following sections).

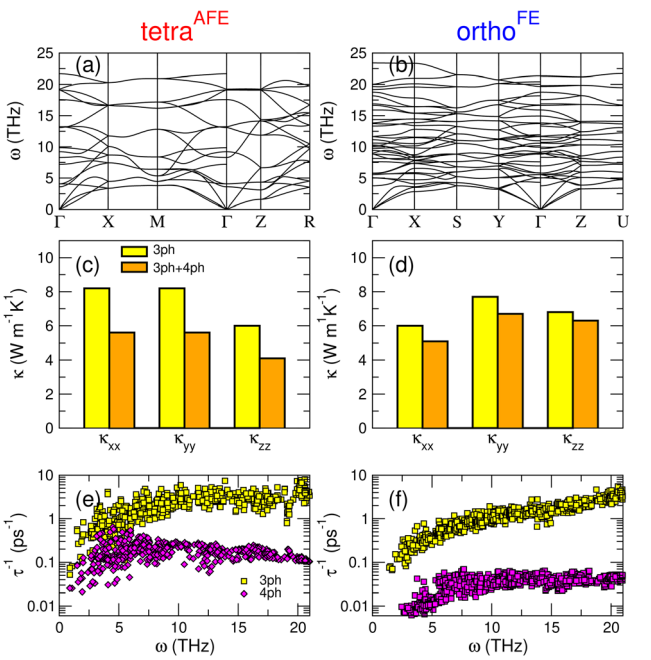

Fig. 1 (a, b) Phonon dispersion, (c, d) thermal conductivity with 3ph and 3ph + 4ph scattering, (e, f) scattering rates of 3ph and 4ph processes for the tetra$^{\text{AFE}}$ (left) and the ortho$^{\text{FE}}$ phases (right).

3.2 Electrophononic switching

We have so far analyzed the Cartesian components of the lattice thermal conductivity for each polymorph of ZrO_2 separately: we now examine the changes associated with the tetragonal-to-orthorhombic phase transition. As explained in the Introduction section, such a transition can be actually driven by an external electric field, as demonstrated experimentally.[10] More importantly, the possibility of a reversible phase transition between these two polymorphs enables electrophononic effects, whereby an electric field modulates the phononic properties of the material. We now want to assess the extent to which this phase transition can modulate the heat transport properties, a modulation that, if sufficiently large, could be exploited in the design of thermal memories[34] or to encode information in phonon-based logic schemes.[4]

As an example, a solid-state thermal switch based on this effect could be implemented in a metal–ferroelectric–metal thin-film geometry, ZrO_2 (or the related $Hf_{1-x}Zr_xO_2$ system[35,36]) acts as a thermal gate. An external voltage pulse, applied *via* the top electrode and exceeding the coercive field, triggers the phase transition and switches the material between the low-conductivity tetragonal state and the high-conductivity orthorhombic state, enabling real-time modulation of the heat flux between the electrodes.

Our results are summarized in Fig. 2(a), where we plot the ratio between the diagonal components of the lattice thermal conductivity of the orthorhombic and tetragonal phases. A very intriguing scenario emerges: κ_{xx} exhibits a slight decrease, whereas κ_{yy} and κ_{zz} increase, with the latter showing a remarkable 53% enhancement. The frequency-resolved k, displayed in panels (b)–(d), indicates that the orthorhombic phase is more conductive than the tetragonal one at low frequencies ($\omega \lessapprox 4$ THz), and this behavior drives the overall enhancement of κ_{yy} and κ_{zz}. For κ_{xx}, this trend is counterbalanced by the mid-frequency range (4 THz $< \omega <$ 12 THz), where the tetragonal phase is more conductive, resulting in an overall 10% decrease shown in Fig. 2(a).

This result is somewhat surprising, as one might expect the orthorhombic phase to be less conductive due to its lower symmetry. Indeed, Fig. 1 shows that it has more phonon bands, as expected from the larger number of atoms in the primitive cell, suggesting a larger number of allowed phonon–phonon processes. This qualitative observation is confirmed by analysis of the weighted phase space available for 3ph and 4ph processes, P_3 and P_4, as shown in Fig. 3(a) and (b), where these quantities account for phonon–phonon collision processes that conserve energy and momentum and are typically negatively correlated with k.[37] Both P_3 and P_4 are larger for the orthorhombic phase at all frequencies, with this difference being especially large for 4ph processes.

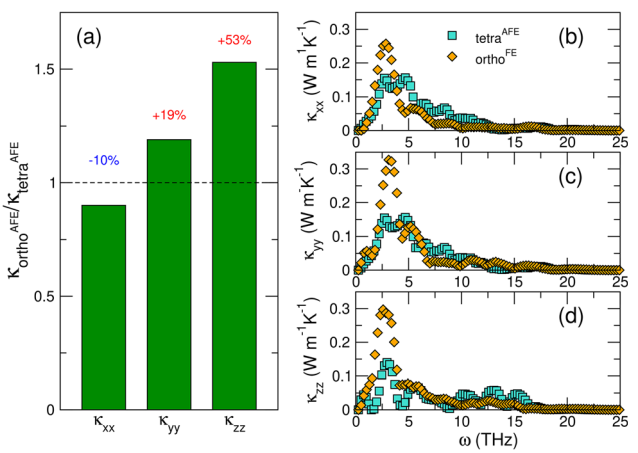

Fig. 2 (a) Variation of the thermal conductivity, $\Delta\kappa = \kappa_{ortho^{FE}}/\kappa_{tetra^{AFE}}$, upon the field-induced tetra^{AFE} → ortho^{FE} phase transition. (b)–(d) Spectral thermal conductivity, $\kappa_{ii}(\omega)$, of the tetragonal and orthorhombic crystal phases.

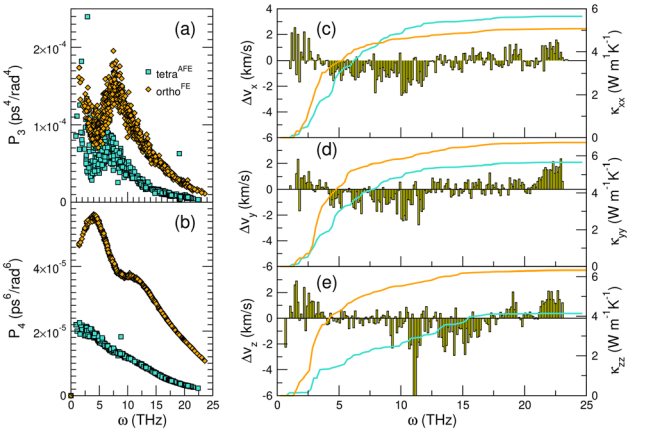

Fig. 3 Phase space for (a) three-phonon and (b) four-phonon processes as a function of frequency. (c)–(e) Difference between the average phonon velocities of the two phases, defined as $\Delta v_i = v_{ortho,i} - v_{tetra,i}$ with $i = x, y, z$, as a function of frequency. Averages were computed over intervals of 0.125 THz. Panels (c)–(e) also display the accumulated thermal conductivity of the tetragonal (turquoise) and orthorhombic (orange) phases as a function of frequency, where $\kappa_{ii}(\bar{\omega})$ represents the thermal conductivity computed by accounting only for phonons with $\omega < \bar{\omega}$.

We also note that phonon group velocities do not account for the observed differences in k. In Fig. 3(c)–(e), we plot the difference between the group velocities of the orthorhombic and tetragonal phases, $\Delta v_i = v_{ortho,i} - v_{tetra,i}$ with $i = x$, y, and z, after averaging over intervals of 0.125 THz (yellow bars). The same panels show the accumulated thermal conductivity of both phases (solid curves). Focusing on κ_{yy} and κ_{zz}, we observe that their larger values in the orthorhombic phase begin to accumulate at $\omega \approx 3$ THz, yet in this region both Δv_y and Δv_z are negative, indicating that the tetragonal phase has larger velocities. For κ_{xx}, when the tetragonal phase becomes more conductive around 8 THz, v_x^{tetra} is indeed larger than v_x^{ortho} (*i.e.*, $\Delta v_x < 0$), which partially contributes to the observed difference.

As result, the observed k values cannot be explained on purely harmonic grounds: (i) the phase space is larger (substantially larger for 4ph processes) for the orthorhombic phase; (ii) phonon velocities are generally larger for the tetragonal phase; (iii) the volumetric heat capacities of the two phases are very similar, with the tetragonal phase being slightly larger (2.84 *vs.* 2.80 MJ m^{-3} K^{-1} at room temperature). All these factors suggest that the tetragonal phase should have a larger k, which contradicts our results where only the moderate change in κ_{xx} follows this trend. In particular, neither the approximately 20% larger value of κ_{yy} nor the approximately 50% larger value of κ_{zz} in the orthorhombic phase can be understood based on harmonic properties alone.

Therefore, the overall increase in k upon the tetragonal-to-orthorhombic phase transition is entirely due to a generalized reduction in scattering rates, *i.e.*, an increase in phonon lifetimes τ. This is clearly illustrated in Fig. 4(a), which shows that the scattering rates for phonon–phonon collisions (including both 3ph and 4ph processes) are uniformly smaller in the orthorhombic phase compared to the tetragonal phase. The situation becomes even clearer in Fig. 4(b), where we first

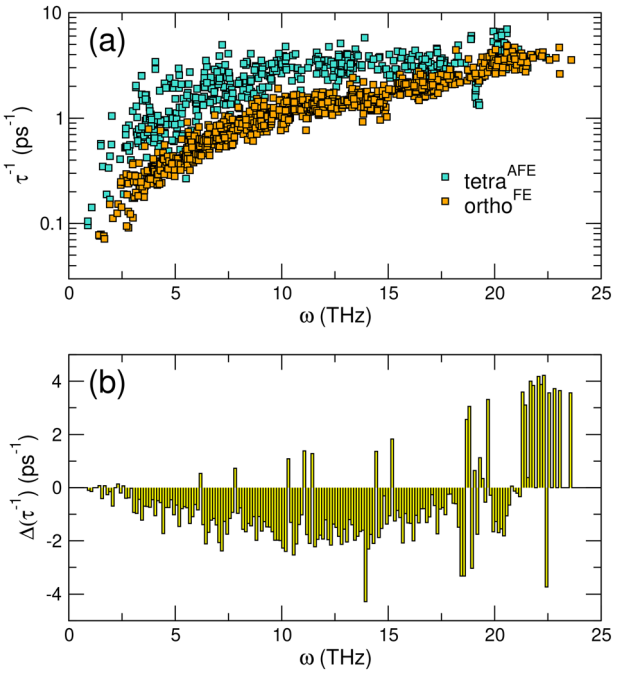

Fig. 4 (a) Total scattering rate, τ^{-1}, for phonon–phonon processes in the tetragonal and orthorhombic crystal phases as a function of frequency. (b) Difference between the average scattering rates of the two phases, defined as $\Delta(\tau^{-1}) = \tau_{ortho}^{-1} - \tau_{tetra}^{-1}$, as a function of frequency. Averages were computed over intervals of 0.125 THz.

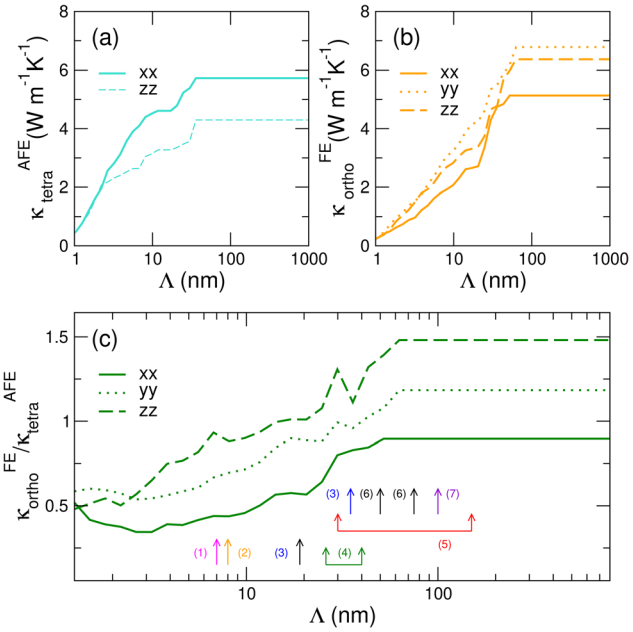

Fig. 5 Accumulated thermal conductivity as a function of the mean free path Λ for (a) the tetragonal and (b) the orthorhombic phase. Here, $k(\bar{\Lambda})$ indicates the value of k when only phonons with $\Lambda < \bar{\Lambda}$ are considered. (c) Ratio between the accumulated values of k^{FE}_{ortho} and k^{AFE}_{tetra} from panels (a) and (b). The arrows indicate the size of experimentally reported ZrO_2 tetragonal crystallites: (1) Solomon *et al.*,[38] (2) Lomenzo *et al.*,[10] (3) Kim *et al.*,[13] (4) Kukli *et al.*,[42] (5) Raghavan *et al.*,[40] (6) El-Shanshoury *et al.*,[41] and (7) Garvie *et al.*[39]

average the scattering rates over frequency intervals of 0.125 THz and then compute the difference $\Delta(\tau^{-1}) = \tau_{ortho}^{-1} - \tau_{tetra}^{-1}$. The difference $\Delta(\tau^{-1})$ is negative at nearly all frequencies, indicating $\tau_{tetra}^{-1} > \tau_{ortho}^{-1}$ and thus greater anharmonicity in the tetragonal phase. Only for $\omega \gtrsim 21$ THz do we find higher scattering rates in the orthorhombic phase, but as shown by the accumulated thermal conductivity in Fig. 3(c–e), phonons in this frequency range contribute negligibly to k.

3.3 Discussion

Beyond the specific case of ZrO_2, our results establish general principles for the design of materials with electrically tunable thermal transport. In particular, field-induced structural phase transitions between polymorphs with markedly different anharmonicity emerge as an effective route to achieve large and reversible modulation of thermal conductivity, provided that the transition significantly alters phonon scattering rates rather than merely harmonic properties such as group velocities or heat capacity. This indicates that promising candidates are systems with strong anharmonicity and multiple competing phases accessible *via* external stimuli such as electric fields, strain, or light. Furthermore, our findings highlight the essential role of higher-order (four-phonon) scattering processes, which can determine not only the magnitude of thermal conductivity but even qualitative trends, thereby requiring computational approaches beyond standard three-phonon treatments. Finally, the dominant contribution of low-frequency phonons with long mean free paths suggests that targeting materials in which these modes are strongly affected across phase transitions offer a particularly effective strategy for maximizing thermal switching.

The intrinsic lattice thermal conductivity discussed above applies to bulk crystalline samples with grain sizes of $d_{grain} \gtrsim 100$ nm, where phonon–phonon scattering dominates. However, in nanostructured ZrO_2, grain boundaries introduce additional scattering that can substantially reduce k. We include this effect through the phonon mean free path (MFP) distribution and cumulative thermal conductivity $\kappa(\Lambda)$,[23] as shown in Fig. 5(a) and (b). The MFP spectrum reveals that approximately 50% of the heat flux is carried by phonons with $\Lambda <$ 20–30 nm in both tetragonal and orthorhombic phases, with near-complete saturation occurring by $\Lambda \sim 100$ nm for the former and $\Lambda \sim 200$ nm for the latter (slightly broader for κ_{zz} in the orthorhombic phase). This distribution effectively set the grain-size dependence of k in polycrystalline specimens.

Interestingly, experimental ZrO_2 microstructures span a wide range. Nanocrystalline samples exhibit crystallite diameters as small as approximately 7 nm, with metastable tetragonal ZrO_2 containing orthorhombic nanodomains (approximately 2 nm correlation length) separated by domain walls.[38] Garvie *et al.*[39] reported larger tetragonal ZrO_2 nanoparticles with diameters of up to 100 nm, while Raghavan *et al.*[40] obtained yttria-stabilized nanocrystalline tetragonal zirconia ranging from 30 to 150 nm. Other works reported tetragonal nanodomains of 19 and 35 nm,[13] 50 and 75 nm,[41] and between 26 and 40 nm.[42]

Our MFP analysis indicates two distinct transport regimes: (a) A nanocrystalline regime ($d_{grain} \lessapprox 30$ nm) where grain boundaries become the dominant scattering mechanism, substantially suppressing k below the intrinsic bulk value. Domain walls in metastable ZrO_2 further enhance scattering, driving the system toward boundary-limited (Casimir-type) transport. (b) A dense polycrystalline regime ($d_{grain} \gtrsim 100$ nm), where only the longest MFP phonons (carrying a small fraction of the total heat flux) are affected by a significant boundary scattering. The measured k value remains close to our calculated intrinsic values, with phonon–phonon and isotope scattering effectively dominating the thermal resistance.

This grain-size dependence enables thermal conductivity engineering: reducing d_{grain} below approximately 30–50 nm affects the majority of heat-carrying phonons, maximizing k suppression. Such nanostructuring is particularly relevant for thermal barrier coatings, where low k is desirable.

We argue that for the field-induced tetragonal ↔ orthorhombic thermal switching, grain boundary scattering has two key implications. First, absolute k values in both phases will decrease in nanostructured samples compared to our bulk predictions. Second, the switching contrast will also be altered because the two phases exhibit different MFP distributions, and thus boundary scattering suppresses k to different degrees in each phase. This effect is illustrated in Fig. 5(c), which shows the ratio $\kappa_{ortho^{FE}}/\kappa_{tetra^{AFE}}$ as a function of Λ, serving as a proxy for the sample size. In the same plot, we indicate the sizes of tetragonal nanodomains reported in the literature, highlighting the possibility of accessing different switching ratios of the field-induced tetragonal–orthorhombic transformation by controlling the sample size.

However, if the domain-wall density differed between the two phases, the switching contrast could deviate from bulk predictions. The orthorhombic phase is stabilized by domain walls that pin ferroelastic distortions.[38] If the field-induced transition alters the domain structure (either refining or coarsening domains), the two phases may experience different effective scattering lengths. The quantitative assessment of this effect will require experimental characterization of the domain configuration before and after the transition (*e.g.*, *via* transmission electron microscopy). Importantly, this consideration does not imply a lack of controllability or practical limitations for nanostructured implementations. In contrast, the experimentally demonstrated reversibility of the phase transition[10] indicates that the domain structure is at least partially recoverable upon cycling, which supports the feasibility of stable and reproducible thermal switching behavior. Furthermore, direct experimental evidence in ZrO_2 thin films (the geometry in which the switching effect is most naturally implemented) supports this expectation: the critical electric fields governing the field-induced tetragonal-to-orthorhombic phase transition are reversibly modulated by field-cycling, with high-field cycling lowering the coercive fields and subsequent lower-field cycling effectively restoring them.[43] Although our calculations address the intrinsic bulk thermal conductivity, this reversible behavior of the switching cycle provides additional and independent support for the possibility to control the domain structure under repeated switching.

We finally observe that while grain boundary scattering reduces absolute k values in nanostructured ZrO_2, the large anisotropic modulation—particularly the approximately 50% enhancement in κ_{zz}—should persist in large crystallites.[39,40] It is important to note, however, that the change in k for smaller nanodomains is not necessarily smaller, but rather different in character. For instance, for the smallest crystallites reported by Solomon *et al.*,[38] we found a decrease of approximately 56% in κ_{xx}, which is substantial and comparable to the approximately 56% increase in κ_{zz} for bulk-like samples.

We conclude our analysis by outlining two possible limitations of our calculations. First, yttria doping is sometimes used to stabilize the tetragonal phase of ZrO_2.[40,44] Its effect on thermal conductivity, which may affect the two phases to different degrees, is not accounted for in our calculations. Second, it remains to be determined which crystallite-size ranges are suitable for realizing in practice the field-induced phase transition considered here. Experimental evidence shows that tetragonal nanodomains up to 100 nm can be synthesized[39]; however, the voltage required to achieve the coercive electric field, E_{coe}, capable of transforming them into the orthorhombic – estimated to be ≈ 1 MV cm^{-1}[10] – phase may be quite large, potentially leading to leakage currents and material degradation issues. If we assume a simple linear relationship, we have that $V = E_{coe}\, d$. In order to avoid dielectric breakdown, V should be smaller than 6 V (being 6 eV the corresponding bandgap value[45]), setting a limit for a d of 60 nm. At this thickness, the 50% change of κ_{zz} is essentially preserved, but lower values d (safer, from the viewpoint of preventing a dielectric breakdown) would yield a different, yet still sizeable, variation of k.

A central motivation of this work is to evaluate the feasibility of electrophononic applications in realistic materials, for which ZrO_2 constitutes a particularly attractive case of study. Electric-field-induced reversible switching between nonpolar and polar phases has been experimentally demonstrated in ZrO_2 thin films.[10,35,43] While direct time-resolved structural measurements are not yet available for pristine ZrO_2, nanosecond and sub-nanosecond polarization-switching experiments in devices based on fluorite-structures HfO_2 and HfO_2–ZrO_2[46] indicate that the underlying lattice transition is intrinsically ultrafast, given the identical displacement-type mechanism. In addition, electric control of phonon-related phenomena in polar materials has been established in recent studies.[47–49] Our calculations predict a sizable and anisotropic modulation of the thermal conductivity, reaching up to $\sim 50\%$, which is comparable to or exceeds values targeted in phononic device applications. Importantly, this effect remains robust when accounting for realistic factors such as nanostructuring and grain-size effects, persisting across experimentally accessible length scales albeit with modified anisotropy. These findings indicate that electrophononic functionality in ZrO_2 is experimentally attainable with current thin-film technologies and, more broadly, that the underlying design principles based on phase-transition-driven changes in

anharmonic phonon scattering can be extended to other complex oxides exhibiting electric-field-induced structural transitions.

4 Conclusions

We have performed a comprehensive first-principles investigation of the lattice thermal conductivity in tetragonal antiferroelectric and orthorhombic ferroelectric phases of ZrO_2 thin films, with particular emphasis on the role of higher-order anharmonicity and thermal transport modulation induced by the field-driven phase transition between these polymorphs. Our calculations, based on the Boltzmann transport equation with phonon–phonon scattering processes up to the fourth order, reveal several key findings with significant implications for thermal management and phononic device applications.

First, we have demonstrated that four-phonon scattering processes are essential for accurately predicting the thermal conductivity of ZrO_2. While the tetragonal phase exhibits a substantial reduction of more than 30% in thermal conductivity when four-phonon processes are included, the orthorhombic phase shows a more moderate decrease of approximately 15% for the in-plane components and less than 8% for the out-of-plane components. Notably, inclusion of four-phonon scattering reverses the relative ordering of thermal conductivities.

Second, we have identified a remarkable electrophononic switching effect associated with the reversible field-induced tetragonal-to-orthorhombic phase transition. The thermal conductivity exhibits highly anisotropic modulation upon switching: while κ_{xx} decreases by approximately 10%, κ_{yy} increases by approximately 20%, and most strikingly, κ_{zz} shows an enhancement of approximately 53%. This large anisotropic response cannot be explained by harmonic properties alone, such as phonon group velocities, phase space for scattering, or heat capacity. Instead, our analysis reveals that the modulation originates entirely from differences in anharmonicity between the two phases, with the tetragonal phase exhibiting systematically higher phonon scattering rates across nearly the entire frequency spectrum.

Finally, we have examined the influence of grain boundary scattering on thermal transport in nanostructured ZrO_2. The mean free path analysis indicates that approximately 50% of the heat flux is carried by phonons with Λ <20–30 nm, defining a nanocrystalline regime where boundary scattering dominates and a polycrystalline regime where intrinsic phonon–phonon scattering prevails. Importantly, the switching contrast between phases varies with grain size due to their different mean free path distributions. For the smallest experimentally reported crystallites (approximately 7 nm), we predict a 56% decrease in κ_{xx} upon phase transition, comparable in magnitude to the 56% increase in κ_{zz} observed in bulk-like samples, demonstrating that substantial thermal modulation persists across length scales, albeit with different anisotropic character.

The giant modulation of k observed here in ZrO_2 aligns with recent findings in other ferroic and phase-change materials, such as antiferroelectric $PbZrO_3$[36] and two-dimensional $MoTe_2$,[50] where the interplay between structural symmetry and higher-order anharmonicity is leveraged for active heat-flow control. Our results indicate that ZrO_2 is a promising platform for electrophononic applications, where electric fields can be used to dynamically control thermal transport. The large, anisotropic modulation of thermal conductivity—particularly the approximately 50% enhancement along the out-of-plane direction in bulk samples—could be exploited in thermal memory devices, phonon-based logic circuits, or adaptive thermal management systems. The persistence of substantial thermal switching effects in nanostructured materials further broadens the potential application space to thin-film and nanocrystalline architectures. Future experimental work should focus on measuring the grain-size-dependent thermal conductivity in both phases, characterizing domain wall configurations before and after switching, and exploring the effect of dopants such as yttria on the switching contrast. The demonstrated reversibility of the phase transition and the purely phononic origin of the thermal modulation suggest that ZrO_2-based electrophononic switches could offer advantages in terms of speed, energy efficiency, and integration with existing ferroelectric device technologies.

Conflicts of interest

There are no conflicts to declare.

Data availability

Data for the thermal conductivity calculations reported in this article are available at Zenodo repository at https://doi.org/10.5281/zenodo.17746932.

Supplementary information (SI) is available. See DOI: https://doi.org/10.1039/d6mh00729e.

Acknowledgements

We thank Wu Li and Carla Verdi for enlightening discussions. We acknowledge financial support from the MCIN/AEI/10.13039/501100011033 under grant PDC2023-145934-I00 and PID2024-162811NB-I00, the Severo Ochoa Centres of Excellence Program under grant CEX2023-001263-S, and the Generalitat de Catalunya under grant 2021 SGR 01519. P.B. acknowledges support from the predoctoral program AGAUR-FI ajuts (2024 FI-1 00070) Joan Oró, which is backed by the Secretariat of Universities and Research of the Department of Research and Universities of the Generalitat of Catalonia, as well as the European Social Plus Fund. C.L. acknowledges support from the Spanish Ministry of Science, Innovation and Universities under an FPU grant. Calculations were performed at the Centro de Supercomputación de Galicia (CESGA) and at the Barcelona Supercomputing Center (BSC) within actions FI-2023-3-0043 and FI-2024-3-0032 of the Red Española de Supercomputación (RES). P.B., C.L. and C.C. acknowledge the Maria de Maeztu

Units of Excellence Programme CEX2023-001300-M funded by MCIN/AEI (10.13039/501100011033).

References

1 I. Zardo and R. Rurali, Manipulating phonons at the nanoscale: Impurities and boundaries, *Curr. Opin. Green Sustain. Chem.*, 2019, **17**, 1–7.

2 M. Terraneo, M. Peyrard and G. Casati, Controlling the Energy Flow in Nonlinear Lattices: A Model for a Thermal Rectifier, *Phys. Rev. Lett.*, 2002, **88**, 094302.

3 B. Li, L. Wang and G. Casati, Negative differential thermal resistance and thermal transistor, *Appl. Phys. Lett.*, 2006, **88**, 143501.

4 N. Li, J. Ren, L. Wang, G. Zhang, P. Hänggi and B. Li, Colloquium: Phononics: Manipulating Heat Flow with Electronic Analogs and Beyond, *Rev. Mod. Phys.*, 2012, **84**, 1045–1066.

5 G. F. Nataf, S. Volz, J. Ordonez-Miranda, J. Íñiguez González, R. Rurali and B. Dkhil, Using oxides to compute with heat, *Nat. Rev. Mater.*, 2024, **9**, 530–531.

6 C. Cazorla, S. Bichelmaier, C. Escorihuela-Sayalero, J. Íñiguez, J. Carrete and R. Rurali, Light-driven dynamical tuning of the thermal conductivity in ferroelectrics, *Nanoscale*, 2024, **16**, 8335–8344.

7 C. Cazorla, C. Escorihuela-Sayalero, J. Carrete, J. Íñiguez González and R. Rurali, Optical Control of the Thermal Conductivity in $BaTiO_3$, *Adv. Funct. Mater.*, 2025, **35**, e2425424.

8 S. E. Reyes-Lillo, K. F. Garrity and K. M. Rabe, Antiferroelectricity in thin-film ZrO_2 from first principles, *Phys. Rev. B:Condens. Matter Mater. Phys.*, 2014, **90**, 140103.

9 J. Müller, T. S. Böscke, U. Schröder, S. Mueller, D. Bräuhaus, U. Böttger, L. Frey and T. Mikolajick, Ferroelectricity in Simple Binary ZrO_2 and HfO_2, *Nano Lett.*, 2012, **12**, 4318–4323.

10 P. D. Lomenzo, L. Collins, R. Ganser, B. Xu, R. Guido, A. Gruverman, A. Kersch, T. Mikolajick and U. Schroeder, Discovery of Nanoscale Electric Field-Induced Phase Transitions in ZrO_2, *Adv. Funct. Mater.*, 2023, **33**, 2303636.

11 R. C. Garvie, Stabilization of the tetragonal structure in zirconia microcrystals, *J. Phys. Chem.*, 1978, **82**, 218–224.

12 H. Kim, P. C. McIntyre and K. C. Saraswat, Microstructural evolution of ZrO_2 -HfO_2 nanolaminate structures grown by atomic layer deposition, *J. Mater. Res.*, 2004, **19**, 643–650.

13 S. K. Kim and C. S. Hwang, Atomic Layer Deposition of ZrO_2 Thin Films with High Dielectric Constant on TiN Substrates, *Electrochem. Solid-State Lett.*, 2007, **11**, G9.

14 R. Materlik, C. Künneth and A. Kersch, The origin of ferroelectricity in $Hf_{1-x}Zr_xO_2$: A computational investigation and a surface energy model, *J. Appl. Phys.*, 2015, **117**, 134109.

15 C. Carbogno, R. Ramprasad and M. Scheffler, Ab Initio Green-Kubo Approach for the Thermal Conductivity of Solids, *Phys. Rev. Lett.*, 2017, **118**, 175901.

16 C. Verdi, F. Karsai, P. Liu, R. Jinnouchi and G. Kresse, Thermal transport and phase transitions of zirconia by on-the-fly machine-learned interatomic potentials, *npj Comput. Mater.*, 2021, **7**, 156.

17 G. Kresse and J. Hafner, Ab initio molecular dynamics for liquid metals, *Phys. Rev. B:Condens. Matter Mater. Phys.*, 1993, **47**, 558–561.

18 G. Kresse and J. Hafner, Ab initio molecular-dynamics simulation of the liquid-metal-amorphous-semiconductor transition in germanium, *Phys. Rev. B:Condens. Matter Mater. Phys.*, 1994, **49**, 14251.

19 G. Kresse and D. Joubert, From ultrasoft pseudopotentials to the projector augmented-wave method, *Phys. Rev. B:Condens. Matter Mater. Phys.*, 1999, **59**, 1758.

20 P. E. Blöchl, Projector augmented-wave method, *Phys. Rev. B:Condens. Matter Mater. Phys.*, 1994, **50**, 17953.

21 J. P. Perdew, A. Ruzsinszky, G. I. Csonka, O. A. Vydrov, G. E. Scuseria, L. A. Constantin, X. Zhou and K. Burke, Restoring the Density-Gradient Expansion for Exchange in Solids and Surfaces, *Phys. Rev. Lett.*, 2008, **100**, 136406.

22 A. Togo, L. Chaput and I. Tanaka, Distributions of phonon lifetimes in Brillouin zones, *Phys. Rev. B:Condens. Matter Mater. Phys.*, 2015, **91**, 094306.

23 W. Li, J. Carrete, N. A. Katcho and N. Mingo, ShengBTE: a solver of the Boltzmann transport equation for phonons, *Comp. Phys. Commun.*, 2014, **185**, 1747–1758.

24 Z. Han, X. Yang, W. Li, T. Feng and X. Ruan, FourPhonon: An extension module to ShengBTE for computing four-phonon scattering rates and thermal conductivity, *Comp. Phys. Commun.*, 2022, **270**, 108179.

25 G. Fugallo and L. Colombo, Calculating lattice thermal conductivity: a synopsis, *Phys. Scr.*, 2018, **93**, 043002.

26 S. Tamura, Isotope scattering of dispersive phonons in Ge, *Phys. Rev. B:Condens. Matter Mater. Phys.*, 1983, **27**, 858–866.

27 C. J. Howard, R. J. Hill and B. E. Reichert, Structures of ZrO_2 polymorphs at room temperature by high-resolution neutron powder diffraction, *Acta Crystallogr., Sect. B:Struct. Sci.*, 1988, **44**, 116–120.

28 A. P. S. Crema, M. C. Istrate, A. Silva, V. Lenzi, L. Domingues, M. O. Hill, V. S. Teodorescu, C. Ghica, M. J. M. Gomes, M. Pereira, L. Marques, J. L. MacManus-Driscoll and J. P. B. Silva, Ferroelectric Orthorhombic ZrO_2 Thin Films Achieved Through Nanosecond Laser Annealing, *Adv. Sci.*, 2023, **10**, 2207390.

29 M. Ko, J. S. Park, S. Joo, S. Hong, J. M. Yuk and K. M. Kim, Direct growth of ferroelectric orthorhombic ZrO_2 on Ru by atomic layer deposition at 300C, *Mater. Horiz.*, 2025, **12**, 565–574.

30 T. Feng, L. Lindsay and X. Ruan, Four-phonon scattering significantly reduces intrinsic thermal conductivity of solids, *Phys. Rev. B*, 2017, **96**, 161201.

31 B. Wei, M. Chai, C. Liu, J. Liu, Y. Li, W. Zhang, Q. Wang, E. Mu, B. Wang, Z. Zhou, C. Lin, X. Chen, M. Hu, Y. Zheng and Y.-H. Lin, Phonon bunching induced strong four-phonon scattering for low lattice thermal conductivity in layered Na_2CoSe_2 O, *npj Quantum Mater*, 2026, **11**, 3.

32 T. Feng and X. Ruan, Four-phonon scattering reduces intrinsic thermal conductivity of graphene and the contributions from flexural phonons, *Phys. Rev. B*, 2018, **97**, 045202.

33 C. Cui, Y. Zhang, T. Ouyang, C. Tang, C. He, J. Li and J. Zhong, Effect of four-phonon scattering on thermal transport of γ -graphyne revealed by atomic cluster expansion, *J. Appl. Phys.*, 2024, **136**, 125107.

34 L. Wang and B. Li, Thermal Memory: A Storage of Phononic Information, *Phys. Rev. Lett.*, 2008, **101**, 267203.

35 R. Ganser, P. D. Lomenzo, L. Collins, B. Xu, L. A. Antunes, T. Mikolajick, U. Schroeder and A. Kersch, Mechanism of Antiferroelectricity in Polycrystalline ZrO_2, *Adv. Funct. Mater.*, 2024, **34**, 2405513.

36 K. Aryana, *et al.*, Observation of solid-state bidirectional thermal conductivity switching in antiferroelectric lead zirconate ($PbZrO_3$), *Nat. Commun.*, 2022, **13**, 1573.

37 L. Lindsay and D. A. Broido, Three-phonon phase space and lattice thermal conductivity in semiconductors, *J. Phys.: Condens. Matter*, 2008, **20**, 165209.

38 A. P. Solomon, E. C. O'Quinn, J. Liu, I. M. Gussev, X. Guo, J. Neuefeind, C. Trautmann, R. C. Ewing, G. Baldinozzi and M. K. Lang, Atomic-scale structure of ZrO_2: Formation of metastable polymorphs, *Sci. Adv.*, 2025, **11**, eadq5943.

39 R. C. iGarvie, R. H. Hannink and R. T. Pascoe, Ceramic steel?, *Nature*, 1975, **258**, 703–704.

40 S. Raghavan, H. Wang, R. B. Dinwiddie, W. D. Porter and M. J. Mayo, The effect of grain size, porosity and yttria content on the thermal conductivity of nanocrystalline zirconia, *Scr. Mater.*, 1998, **39**, 1119–1125.

41 I. A. El-Shanshoury, V. A. Rudenko and I. A. Ibrahim, Polymorphic Behavior of Thin Evaporated Films of Zirconium and Hafnium Oxides, *J. Am. Ceram. Soc.*, 1970, **53**, 264–268.

42 K. Kukli, M. Ritala, J. Aarik, T. Uustare and M. Leskelä, Influence of growth temperature on properties of zirconium dioxide films grown by atomic layer deposition, *J. Appl. Phys.*, 2002, **92**, 1833–1840.

43 J. Shin, D. H. Shin, K. Do Kim, H. Seo, K. H. Ye, J. W. Jeon, T. K. Kim, H. Paik, H. Song, S. H. Lee, J.-H. Choi and C. S. Hwang, Reversible modulation of critical electric fields for a field-induced ferroelectric effect with field-cycling in ZrO_2 thin films, *J. Mater. Chem. C*, 2024, **12**, 15423–15434.

44 M. Nagai, Y. Higashitani, M. Ashida, K. Kusakabe, H. Niioka, A. N. Hattori, H. Tanaka, G. Isoyama and N. Ozaki, Terahertz-induced martensitic transformation in partially stabilized zirconia, *Commun. Phys.*, 2023, **6**, 88.

45 R. H. French, S. J. Glass, F. S. Ohuchi, Y. N. Xu and W. Y. Ching, Experimental and theoretical determination of the electronic structure and optical properties of three phases of ZrO_2, *Phys. Rev. B:Condens. Matter Mater. Phys.*, 1994, **49**, 5133–5142.

46 M. Si, X. Lyu, P. R. Shrestha, X. Sun, H. Wang, K. P. Cheung and P. D. Ye, Ultrafast measurements of polarization switching dynamics on ferroelectric and anti-ferroelectric hafnium zirconium oxide, *Appl. Phys. Lett.*, 2019, **115**, 072107.

47 P. Upreti, D. Rashadfar, R. Sahul, D. L. Abernathy, J. P. Heremans, R. P. Hermann and M. E. Manley, Electric Field Control of Phonon Lifetimes and Thermal Conductivity in Relaxor-Based Ferroelectric. *PRX*, *Energy*, 2026, **5**, 013001.

48 C. Liu, *et al.*, Low voltage-driven high-performance thermal switching in antiferroelectric $PbZrO_3$ thin films, *Science*, 2023, **382**, 1265–1269.

49 B. L. Wooten, R. Iguchi, P. Tang, J. S. Kang, K. Ichi Uchida, G. E. W. Bauer and J. P. Heremans, Electric field-dependent phonon spectrum and heat conduction in ferroelectrics, *Sci. Adv.*, 2023, **9**, eadd7194.

50 Z. Chang, N. McIntosh, Z. Liu and R. Rurali, Giant Thermal Switching via Phase Transition in $MoTe_2$, *J. Phys. Chem. Lett.*, 2026, **17**, 1262–1270.